DIRECT THERMAL WATER SPLITTING BY CONCENTRATED SOLAR RADIATION FOR HYDROGEN PRODUCTION

Phase 0:

Proof of concept experiment

FINAL REPORT

by

P. Genequand

This work was conducted pursuant to an Interagency Agreement between the Department of Energy (DOE) and the National Aeronautics and Space Administration (NASA) and in furtherance of work under Prime Contract NAS7-100 between NASA and the California Institute of Technology

JPL Contract No. 955277

June 1980

BATTELLE
Geneva Research Centers
7, route de Drize
1227 Carouge-Geneva
Switzerland

"This report contains information prepared by Battelle-Geneva under JPL sub-contract. Its content is not necessarily endorsed by the Jet Propulsion Laboratory, California Institute of Technology, or the National Aeronautics and Space Administration".

TABLE OF CONTENTS

EXECUTIVE SUMMARY

BACKGROUND

Among the many methods for producing hydrogen from water those which convert solar energy directly into hydrogen are of particular interest. In fact, hydrogen produced by solar reactors in remote locations can be stored and transported economically through pipelines to other locations. Such a technology would, therefore, constitute an ideal energy storage - conversion system whereby the storage vector hydrogen can be used at the same time in chemical, physical, and in thermal applications, e.g. both for mechanical energy generation (transportation) and for heating purposes. Also the further conversion of hydrogen into electric energy by means of fuel cells or combined cycle plants can be envisaged.

Direct thermal water splitting - a most simple and thus desirable technology for converting solar energy into hydrogen - needs higher temperatures than any other proposed water splitting process and also needs a technical concept which allows for suitably high cycle efficiencies. The special concept proposed by Battelle should render it possible to work at relatively low temperatures of the order of 2500°K; one can therefore use materials which at higher temperatures would loose their otherwise unsatisfactory mechanical and chemical stability.

The proposed technical concept which satisfies the above requirements is based upon a low pressure water splitting cycle (0.1 atm) and upon the separation of the dissociation components: H, H_2, O, OH by Knudsen effusion through a porous refractory membrane.

In contrast to an earlier concept proposed by Fletcher [4], the Battelle design of the membrane consists of porous tubes of thoria or zirconia whereby the dissociated water vapor diffuses from the outside to the inside of the tubes so that the porous wall material is subjected only to pure compressional stresses

of the order of 0.3 kg/cm^2. The tubes should therefore be able to withstand the mechanical stress at the operating temperature of approximately 2500°K without significant creep.

Apart from the mechanical and chemical stability of the separation membrane, the collection yield of the solar concentrator as limited by radiation losses must be considered. The proposed reduction of operating temperature and pressure will alleviate the radiation loss problem considerably. Calculations show that an overall solar conversion yield of 40% can be expected for the production of H_2 compressed to 100 atm, and this with cooling requirements as low as 25%.

STUDY PERFORMED

This report presents the results of the first successful experimental demonstration of direct thermal water splitting obtained within a four-month project carried out under contract for the Jet Propulsion Laboratory.

The concentrated solar energy input to the water splitting reactor was simulated by radiative heating from a CO_2 laser beam. Water vapor was introduced into the reaction chamber in which a separation membrane in the form of a small disc of porous ZrO_2 had been arranged. The dissociation products were monitored by a mass spectrometer. Because of limited time and resources the experiments could not be conducted at a constant vapor pressure of 0.1 atm. In order to overcome this limitation a special thermostat would have to be built around the reactor vessel so as to maintain a temperature of about 45°C and (without condensation) a vapor water pressure of 0.1 atm. The conclusions of this report are, therefore, based on experimental conditions which in terms of the operating pressure are not yet optimal.

Mass-spectrometric measurements show that water vapor was dissociated with a dissociation degree of the order of 30% at 2600°K at a total pressure of 0.18 Torr. These results are compatible with the theoretical predictions: hydrogen and oxygen from the dissociation reaction can be separated through a ZrO_2 porous membrane in the proportion given by the Knudsen effusion regime. The experimentally observed separation yield between hydrogen and oxygen appears even to be higher than theoretically predicted.

CONCLUSIONS

The following conclusions can be drawn as regards the direct thermal water splitting process as experimentally demonstrated for the first time in this phase zero program:

- The conceptual study indicates that an industrial reactor for the production of hydrogen by direct thermal water splitting would have an overall useful yield of 40% of the collected solar energy with cooling requirements as low as 25%. This presupposes that water vapor can be dissociated at 2500°K under a total pressure of 0.1 atm with a dissociation degree of 10% and that the reaction products can be flowed at high temperature through a porous membrane under a Knudsen effusion regime.

- The experimental demonstration has shown that direct thermal water splitting can be successfully carried out yielding a dissociation degree of about 30% at 2600°K under a total pressure of 0.18 Torr. The experiments have also shown that hydrogen and oxygen can be separated by means of a porous ZrO_2 membrane in the proportions of a Knudsen effusion regime.

- The process efficiency measured still needs to be compared with the theoretical values calculated. Owing to time and budget limitations it has not been possible to operate the experimental reactor at the total pressure of 0.1 atm. This would have required to maintain the reactor temperature at about 45°C by means of an appropriate thermostat in order to avoid water vapor condensation. Further work should, therefore, be conducted including experiments at various total pressures of up to 0.1 atm.

- The work carried out has also given evidence on the problems associated with the preparation and use of porous ceramic membranes in the reactor for hydrogen-oxygen separation. The fact that the membranes must withstand strong chemical and mechanical constraints at rather high temperatures indicates that considerable further work must be done in order to optimize the membrane preparation process.

It should be emphasized that during this phase zero program of four-month duration, substantial time had to be devoted to the setting up of the rather sophisticated experiment. The objective of the JPL sponsored phase zero to conduct a proof of principle experiment in support of the conceptual study carried out on Battelle internal funds was successfully achieved.

RECOMMENDATIONS

The experiments conducted in the framework of this program as well as the conceptual study show that the process of direct thermal water splitting has a potential for hydrogen generation from solar energy. In particular, the new concept for the separation membrane will allow for operating temperatures around or below 2500°K. Thereby, the problem of reactor materials stability and efficiency losses in the solar concentrator are largely alleviated.

It is recommended that the experiments undertaken during the present work be continued and expanded in order to operate the reactor under the following conditions:

- Variation of the total pressure up to a few torrs (first phase) and up to 0.1 atm (second phase)
- Use of porous membranes for the H_2/O_2 separation based on ThO_2 and improving the preparation processes for ZrO_2 as well as for ThO_2
- Introduction of a more accurate temperature measurement instrumentation for the hot spot
- Providing for a more accurate partial pressure calibration so as to allow for independent determination of the dissociation degree and of the reaction production separation.

A middle-term application for the direct production of solar hydrogen in lands situated between 20° and 40° latitude should be envisaged. To achieve this goal it is recommended to develop a 15 kW solar direct water splitting reactor. As a first step towards this goal a program should be established which identifyes the required effort in time and resources and the various problem areas to be tackled.

ABSTRACT

The direct production of hydrogen from water and solar energy concentrated into a high temperature aperture is considered. A key item is shown to be the development of an efficient solar powered reactor able to dissociate water vapor and to separate the reaction product (hydrogen and oxygen) at this high temperature.

In support of a conceptual study, the first experimental demonstration of direct water splitting has been successfully achieved by means of a laboratory reactor assembled and tested in the framework of a four-month project.

The inputs of this reactor are water vapor and radiative heating from a CO_2 laser; the outputs are water vapor enriched in hydrogen and water vapor enriched in oxygen.

The separation membrane is a small disc of porous ZrO_2 heated up into the temperature range of 1800°K to 2800°K. During operation, the reacting water vapor has been observed to be dissociated and the reaction products separated in the proportions foreseen by the conceptual study.

The total pressure within the reaction chamber has been limited to 0.15 Torr for technical reasons (to avoid water vapor condensation within the reactor). A few modifications in the set-up would enable the reactor to be operated at an increased pressure of a few Torrs. More substantial modifications would allow for a reaction pressure of the order of 0.1 atm, which is considered to be a normal operation pressure for an industrial reactor.

A middle-term application for the direct production of solar hydrogen in desertic lands situated between 20° and 40° latitude is envisaged; first industrial pilot plants can be expected to be initiated toward 1990 if a proper effort is made.

DIRECT THERMAL WATER SPLITTING BY CONCENTRATED SOLAR RADIATION FOR HYDROGEN PRODUCTION

Phase 0:

Proof of concept experiment

FINAL REPORT

by

P. Genequand

---

1. INTRODUCTION

1.1 HYDROGEN PRODUCTION SCHEMES

The production of hydrogen from solar energy will be of considerable interest in a few years, especially in areas supplied with plenty of solar energy, but where the development of electricity distribution networks makes no economical sense, such as in low latitude deserts. Hydrogen produced by solar reactors in these otherwise valueless lands could be stored and transported through pipelines or combined with carbon dioxide to give methanol or other transportable fuels.

The various proposed schemes can be classified according to the working temperature of the cycle considered. In the low temperature range the solar thermal electricity-water-electrolysis concept ($T \sim 600°-800°K$) is located. In the intermediate range the various thermochemical cycles ($T \sim 1000°-2000°K$) are located and in the high range the direct thermal splitting of water ($T \sim 2500°-3500°K$) is found.

Water electrolysis from thermal (or from photovoltaic) solar electricity is a hybrid solution. The technology involved is complex but already well-known

and could be applied without major difficulty. Owing to the low cycle temperature, the solar concentrators will be relatively inexpensive and usable even in regions where the solar supply is suboptimal and somewhat irregular. In this latter case the hydrogen produced will mainly constitute a buffer storage to allow the power plant to feed regular power into an electrical network. However, its complexity and low overall efficiency render this firstsolution uneconomical and particularly inadequate in the hot deserts (owing to the high cooling requirements).

Several chemical cycles adapted to hydrogen production have been identified and studied. Owing to their higher working temperatures, higher cycle efficiencies and also lower cooling requirement can be achieved. The technology remains still to be developed but is potentially simpler than that used for the water electrolysis scheme.

Direct thermal splitting of water is the simplest concept, since the only chemical involved is water itself. It corresponds also to the highest cycle yield, whence the lowest cooling requirements. However, this concept has not been taken very much into consideration because it has generally been admitted that a satisfactory splitting yield can be achieved only at temperatures in excess of 3000°K [1].

At such high operation temperatures, a major problem is to find reactor materials endowed with sufficient mechanical and chemical stability. Another difficulty is that the collection yield of the best solar concentrators, such as the 1 MW solar furnace at Odeillo [2] does not exceed 60% at 3000°K owing to the thermal reradiation losses from the hot reactor aperture. This would severely limit the overall efficiency of the cycle.

1.2 DIRECT THERMAL WATER SPLITTING

In recent years it has been realized that efficient direct water splitting schemes could be envisaged at a considerably lower operation temperature (of the order of 2500°K). The solar collection yield can then be expected to reach 80% and candidate reactor materials can be found (ThO_2, ZrO_2).

The proposed schemes are generally based on a low pressure cycle (0.1 atm) and a relatively low dissociation degree (10%) in the reaction chamber. According to the laws of thermochemistry, the dissociation degree of water vapor is 9% at 2500°K and 0.1 atm [3]. The main problem in all these schemes is presented by the separation of the dissociated components H, H_2, O, OH at the necessarily high temperatures.

Fletcher [4] has described a process based on Knudsen effusion through a porous refractory membrane. In this flow regime the effusion rate is proportional to $1/\sqrt{M}$, where M is the molecular or atomic mass. Thus hydrogen, being lighter than oxygen, will diffuse in excess through the membrane. By recombination and condensation of the water vapor during cooling of the effusates, hydrogen and oxygen can be completely separated and extracted. According to Fletcher, efficient operation should, in principle, become possible at temperatures as low as 2200°K.

However, his analysis does not take into account the irreversibility losses associated with the low pressure cycle. This point has been considered by Nakamura [5] who concludes that a low pressure design would have an overall efficiency limited to about 10%, owing to frictional losses within the pumps. However, the friction values used in his estimates have been set much too high (of the order of 100 Joule/liter, which is valid for high vacuum sliding vane pumps). Other pumps like Roots pumps, having a lower compression ratio, exhibit much less frictional losses (1 to 10 Joule/liter) [6]. Non-volumetric pumps (turbines) could also be envisaged for large industrial realizations.

Further approaches based on selective diffusion through compact membranes have been proposed by Ihara [8] for solid diffusion of hydrogen and by Fally [9] for activated solid diffusion of oxygen.

It appears that solid diffusion schemes will be more difficult to reduce to practice than porous wall diffusion schemes, because the membranes must not only withstand the severe mechanical and chemical constraints at the high reaction temperature, but also be able to diffuse about 10^{-4} mole H_2/cm^2s.

This high numerical value for the rate of diffusion can be derived from the following considerations:

The dissociation reaction takes place within a blackbody cavity fitted with an opening of typically 50 cm^2; the solar radiation is concentrated to 1000 W/cm^2 within this aperture. The selective membrane for hydrogen separation in the reactor cavity can have an active area of 1000 cm^2. The equivalent incident power on the selective membrane is thus at least of the order of 50 W/cm^2. The expected overall yield of the reactor for hydrogen production is 40%. The membrane must thus be able to effuse a hydrogen equivalent of 20 W/cm^2, which corresponds to 10^{-4} mole H_2/cm^2s at 0.1 atm (20 cm^3 H_2/cm^2s) which is extremely high value.

One of the best materials for hydrogen permeation is palladium (10^{-2} cm^3/cm^2s at 800°K through 1 mm thick wall, at 0.1 atm). The permeation through nickel reaches 10^{-2} cm^3/cm^2s at 1500°K [10]. Permeation rates through oxides like SiO_2 have much lower values (10^{-6} cm^3/cm^2s at 1500°K).

In the following the rate of molecular effusion across a porous wall is estimated.

Knudsen's expression for the molecular flow along a circular tube is given by [11]:

$$\frac{dn}{dt} = \frac{4\ r^3}{3\ L}\sqrt{\frac{2\ \pi}{MRT}}\ \Delta p \qquad (1)$$

where r is the radius of the tube
L is the length of the tube
Δp is the pressure difference
dn/dt is the flux in mole/s.

Assimilating the porous wall to a regular array of tubes of radius equal to the average pore radius, the following approximative expression for the flux is obtained:

$$\frac{dn}{dt} = \frac{8}{3}\frac{r\ S\ \varepsilon\ \Delta p}{L\ \sqrt{2\pi MRT}} \qquad (2)$$

where S is the surface of the wall
L is the thickness of the wall
ε is the porosity fraction
r is the average pore radius.

Taking $r = 2.10^{-5}$ m
$L = 2.10^{-3}$ m
$\varepsilon = 0.2$
$M = 2.10^{-3}$ kg/mole
$\Delta p = 0.1$ atm $= 10^4$ Pascal
$S = 10^{-4}$ m^2
$T = 2500°K$
$R = 8$ J/°K,

$dn/dt = 1.5.10^{-4}$ mole H_2/cm^2s.

This value is in good agreement with the flow rate requirement mentioned above.

Starting from these considerations, the Battelle-Geneva Research Centre for Industrial Technology has proposed a design for direct water splitting at low pressure (0.1 atm, 2500°K) in which hydrogen and oxygen are separated by Knudsen effusion across a porous wall [12].

This design is similar to the concept proposed by Fletcher, insofar as the basic operating principles are concerned. However, the approach for the porous membrane is quite different. Fletcher proposes to use a thin mesh of thoria cloth [7] comparable to the incandescent mantles of Coleman lamps. It is not shown how this mesh could withstand the mechanical stresses induced by the pressure gradient at the operating temperature.

The Battelle design is based on porous tubes of thoria or zirconia, with a wall thickness of about 2 mm and a diameter of the order of 10 mm. The dissociated water vapor diffuses from the outside to the inside of the tubes, so that the porous wall material is subjected only to a pure compressional stress of the order of 0.3 kg/cm^2.

From values of the creep rate as a function of stress and temperature given by Fulrath [13] a creep value of less than 10^{-3} hr^{-1} can be extrapolated. This shows that the effusion tubes should be able to withstand the required mechanical stress at the projected operating temperature.

The Battelle technical note [12] describes a first-order theoretical derivation which takes into account the solar collection efficiency, the dissociation and separation efficiencies, the irreversible losses in the heat exchangers and the compression work to supply the extracted hydrogen under a pressure of 100 atm.

The resulting energy balance can be summarized as follows:

- absorbed within reflectors 15%
- reradiated to space 20%
- rejected at low temperature 25% (cooling requirement)
- available as H_2 40% (useful yield).

The reradiated energy fraction has been calculated to 20% for a temperature of about 2500°K. Higher temperature in the reactor would significantly increase the radiation losses.

In conclusion it can be said that direct water splitting is linked to two major problems:

- mechanical and chemical stability of the reactor walls (separation membranes)
- collection yield of the solar concentrator.

These problems can be alleviated by a reduction of the pressure and temperature of operation.

A good potential for reduction to practice is presented by the proposed design which is based on a blackbody cavity for the dissociation chamber and on Knudsen effusion through porous refractory tubes for the separation of hydrogen and oxygen. An overall yield of 40% can be expected for the production of H_2 at 100 atm, with cooling requirements as low as 25%.

1.3 EXPERIMENTAL REACTOR

A research proposal for a preliminary experimental (proof-of-concept) phase has been submitted by the Center of Industrial Technology of Battelle-Geneva to the Jet Propulsion Laboratory in Pasadena (California).

As a result, a four-month project (from February 26 to June 28, 1979) has been awarded, during which a laboratory reactor has been assembled and operated.

The main objective of this preliminary phase was to operate this reactor with water vapor and radiative heating as an input and with water vapor enriched in hydrogen and water vapor enriched in oxygen as an output.

The proposed approach was to heat a small disc of porous ThO_2 or ZrO_2 by means of a CO_2 laser beam. The disc was placed on top of a compact ZrO_2 tube situated inside a vacuum vessel, in such a manner as to delimit two compartments separated by the disc.

Water vapor was fed by a microleak into one of the compartments, while both chambers were evacuated by means of sliding vane pumps. During operation, the expected H_2 or O_2 pressure rise in the appropriate compartments were monitored by a mass spectrometer.

It was initially foreseen to operate the reactor at a pressure of 0.1 atmosphere but this has not been possible during this short experimental phase for the following reasons:

- In order to maintain a water vapor pressure of 0.1 atm without condensation the vessel temperature should be held higher than 45°C [14] which means that a special thermostat would have to be built and adapted to the vessel for this purpose.

- A germanium flat has been selected as a window for the introduction of the CO_2-laser beam into the vessel. It is known that this material is subject to

thermal runaway if its temperature exceeds 40°C [15]. Taking into account that during operation of the reactor the power absorbed in the refractory sample can be in excess of 100 W, it is thus necessary to cool the vessel to avoid getting too close to the germanium runaway temperature. In the absence of a special thermostat, the vessel has been fitted with a cooling jacket for circulation of cold water (temperature range 10°C to 15°C). This limits the maximum admissible water pressure within the vessel to less than 0,01 atm.

. Pirani gauges have been selected as the best total pressure monitor within the range 0 to 0.01 atm. It turned out that the useful range of the immediately available instruments was limited to 0.001 atm.

Under these conditions, and to avoid introducing too much water into the sliding vane pumps, the reactor was finally operated at a total water vapor pressure of 0.0002 atm (150 μ Hg).

The influence of this reduced operation pressure on the fraction α of dissociated water vapor, as a function of temperature should now be considered.

This question has been discussed extensively by Dorsey [3]. α is given by:

$$\alpha^3 = (1 - \alpha)^2 \quad (2 + \alpha) \quad (KRT/P) \qquad (3)$$

where K is the constant of dissociation in mole/liter
R = 8.3 . 10^{-2} atm liter/mole (°K)
P is the total pressure, in atm
T is the absolute temperature, in °K.

Table 8 of [3] gives K(T) and α(P,T) in the range 1000°K to 5000°K and 0.1 atm to 100 atm. Using the above expression (3), this table has been completed for the total pressure P = 0.0002 atm. The results are listed in Table 1 and are graphically represented in Fig. 1.

Experimental values for the dissociation fraction α(T), as measured during the present work, have also been reported in Fig. 1.

TABLE 1 - DISSOCIATED FRACTION α FOR H_2O AS A FUNCTION OF PRESSURE AND TEMPERATURE

T [°K]	K(T) [mole/liter]	α(T) [%] at 100 atm	at 0.1 atm	at 0.0002 atm
1 000	$1.09 \cdot 10^{-22}$	0.0000056	0.000056	0.000448
1 500	$3.33 \cdot 10^{-14}$	0.00434	0.0434	0.346
2 000	$5.96 \cdot 10^{-10}$	0.125	1.24	9.42
2 500	$1.89 \cdot 10^{-7}$	0.914	8.77	49.8
3 000	$7.26 \cdot 10^{-6}$	3.24	27.7	84.5
3 500	$7.71 \cdot 10^{-5}$	7.34	51.1	95.1
4 000	$3.43 \cdot 10^{-4}$	12.2	67.8	97.5
4 500	$7.98 \cdot 10^{-4}$	16.5	76.6	98.5

It can be seen that, for a value α = 15%, (a reasonable choice for an industrial reactor) the theoretical dissociation temperature would be 2100°K at 0.0002 atm and 2700°K at 0.1 atm.

Experimentally, this α-value at 0.0002 atm is obtained at 2350°K, thus 250°K higher than expected. This may be due to the low accuracy of the temperature estimate (see section 4.1) but a more fundamental reason can be recognised for this discrepancy. It must be noted that the theoretical values are valid for a reaction in a state of thermal equilibrium. This is not the case of our laboratory reactor, where H_2O is dissociated in a small volume extending a few mm over the hot spot (area 0.5 cm^2, corresponding to the cross-section of the laser beam), while recombination in the temperature range 500 to 2000°K occurs in a much larger volume.

The constant of dissociation $K = k_1/k_2$ should now be considered where k_1 is the dissociation rate and k_2 the combination rate. These rates will be affected by respective variations of the dissociation and the recombination volumes. An increase of the recombination volume will also increase the effective recombination rate k_2, so that K will be proportionally lowered. This corresponds either to a lower total pressure (at a given α and T) or to a higher reaction temperature (at a given α and P) than theoretically expected.

The experimental curve in Fig. 1 lies about half-way between the theoretical curves for P = 0.0002 atm and P = 0.1 atm, thus corresponding to a theoretical pressure of 0.004 atm, which is about 20 times the real pressure (for a given temperature). If this result is interpreted as an effect of the ratio of the recombination to the dissociation volume and if the dissociation volume is admitted to be 0.5 cm^3, then a value of 10 cm^3 for the recombination volume is found which is well in agreement with the actual geometry of the experimental reactor.

1.4 APPLICATION AREAS AND FUTURE DEVELOPMENTS

Two general application areas for solar production of hydrogen by direct thermal water splitting are currently considered at Battelle.

1.4.1 TERRESTRIAL APPLICATIONS FOR DESERTIC LANDS SITUATED BETWEEN 20° and 40° LATITUDE IN BOTH HEMISPHERES

This is a middle-term development. A first four-year program should lead towards a 15 kW-solar experimental reactor. As the end-item of a second four-year program, a prototype of an autonomous hydrogen production plant should be constructed and enter the operational stage. This plant would be in the 360 kW-solar range and comprise 24 reactors of 15 kW each, distributed around one central station (pumps and low-temperature system). Together with the development of this prototype plant the experimental solar reactor would be scaled-up to 40 kW so as to match it with the characteristics of the heliostat tracking platforms developed otherwise for central receiver power plants [16].

Based on these two programs first industrial realizations could be initiated towards 1990 provided an adequate R & D effort is committed to the entire project.

Industrial direct water splitting plants would be characterized by a flexible and modular design: autonomous hydrogen production units of 1000 kW-solar power, each unit including 24 high temperature reactors. The individual 40 kW solar parabolic dish concentrators would use economic tracking platforms similar to those developed for heliostats in large solar central receiver systems.

1.4.2 SPACE ENGINEERING POWER APPLICATIONS

This is a longer term development. In the course of the Battelle conceptual study, it has been realized that direct water splitting at high temperatures has a potential for very high power/weight ratios. This qualifies it as a candidate for solar power via satellite [17] or as a prime energy source for large inhabited space colonies [18].

Design for spatial applications would include central receivers and very large lightweight concentrating structures. First industrial realizations might be initiated towards the year 2000.

2. EXPERIMENTAL SET-UP

The experiment has been built up inside a vacuum testing vessel, which is divided into two compartments by the test sample (porous refractory disc placed on top of a refractory tube). The main volume of the vessel constitutes the upstream section while the inside of the refractory tube below the sample functions as the downstream section. The layout of the vessel and the associated peripheral devices is represented in Fig. 2.

To heat the sample to the desired high temperatures, a DC power CO_2 laser has been installed. It is a folded dual tube device assembled at Battelle-Geneva and operated with a 85% He/5% CO_2 10% N_2 mixture.

The smooth control of the maximum 200 W beam power is provided by a special chopper which has been built to intercept 0 to 100% of the beam by means of a continuous linear position adjustment. The power level of the beam is measured by means of a hand-held laser power probe (Oriel, model 25-B).

After passing through the chopper the laser beam is reflected by an infrared mirror (polished copper disc coated with an evaporated gold layer) and directed down into the test vessel. Not shown in Fig. 2 is a protective graphite disc that can be held above the vessel to arrest the laser beam.

On top of the test vessel a germanium flat (coated with antireflex layers optimized at 10.6 μ) serves as window for the laser beam. In addition to the port hole for the laser beam, the vessel has been provided with an optical window (pyrex flat) for direct observation of the sample. This is necessary for the visualisation of the hot spot on the test sample. The diameter of the laser beam when operating under normal monomode conditions is of the order of 8 mm. The optical window can also be used for pyrometric temperature measurements.

In the upper part of the upstream section, an adjustable Balzers RNV 10 H microleak (H_2O microleak) connects the vessel to a H_2O water supply. A flexible strip heater has been provided to avoid any condensation in the region of the microleak. The test vessel has also been fitted with a water cooling jacket to avoid undue heating during operation with the laser beam.

The lower part of the upstream section is connected to a first 2-stage sliding vane pump (1 m^3/hr) while the downstream section is connected to a second sliding vane pump (5 m^3/hr). With a 25 mm diameter ceramic sample placed on top of the ZrO_2 refractory tube, the pumps are able to maintain a pressure ratio of about 3 between the two compartments.

Both compartments are equipped with total pressure readings (hot wire Pirani gauges), which allow for monitoring total pressures in the range from 10^{-2} Torr (residual pressure before introduction of H_2O) up to a few Torr. The effective working pressure during operation has been set at 0.15 Torr in the upper compartment, yielding a pressure of 0.06 Torr in the downstream compartment.

The ceramic disc is not sealed to the refractory tube, so as to permit easy replacement of the sample without damaging the tube. Under these conditions, part of the effusion from the upstream to the downstream section takes place across the pores of the sample and part through leakage between the sample and the tube. In the pressure range of the experiment, the mean free path is greater than 1 mm and thus both effusion processes obey Knudsen law and contribute to the separation of hydrogen and oxygen.

The composition of the gas within the upstream and the downstream compartments can be monitored alternatively by means of a QUAD analyser (250 RGA of EAI, Palo Alto, Ca.). The available system includes an electron multiplier ion detector (14 stage Cu-Be with internally mounted resistors) and a thoriated irridium filament cathode. The QUAD is connected to its own a vacuum system which includes an Orbitron pump (titanium sublimation pump), a high vacuum ionization gauge (BAG), an isolation valve and a conventional ultrahigh vacuum unit with a zeolit trap and a Hickmann diffusion pump.

The admission of the gas to be monitored by the QUAD is controlled by a precision microleak (Varian 951-5100). The flow rate through this microleak is in the range 10^{-6} to 10^{-8} Torr liter/s which is several orders of magnitude lower than the flow rate through the upstream or the downstream sections; it cannot therefore influence the pressure balance within the reactor.

Two rough vacuum valves allow for the switching from the upstream compartment to the downstream compartment. This operation can be carried out without affecting the microleak adjustment; the relative partial pressures within both compartment can thus be directly compared.

Fig. 3 is a photograph of the actual set-up. On top, to the left, is the front panel of the laser. On top, towards the middle, is the chopper. Below in the middle the testing vessel can be seen. To the right, in the foreground is a disused QUAD head; the active QUAD head is visible to the extreme right of the picture, with the label "ONE". The T connection to the Varian microleak can be seen on the lower right side. Below the laser panel, the small instrument with a dial is the Oriel 25-B power-probe.

Fig. 4 is a photograph of a ZrO_2 porous disc on top of the ZrO_2 compact tube. The picture shows an arrangement of three stainless steel rods which maintain the sample in its place. The sample shows a central white spot where it has been heated by the laser beam. The surrounding region (heated at intermediate temperatures) is white-grey. The rim of the disc which remains in the coldest region is black (excess of metallic deposits accumulated during vacuum sintering).

3. SAMPLE PREPARATION

ZrO_2 and ThO_2 porous discs have been prepared. Owing to time and budget constraints, this part of the work has been strictly limited to what was necessary to make the reactor work.

3.1 MATERIAL SELECTION

The need for chemical stability towards H_2O and its dissociation products at temperatures of the order of 2500°K dictates the use of a stable oxide with the highest possible free energy of formation per mole of oxygen. Mechanical and lifetime constraints impose the requirement of the highest possible melting and boiling points. These properties have been compiled from [19], [20], [21] for oxides with melting point above 2500°K and are summarized in Table 2.

TABLE 2 - STABLE REFRACTORY OXIDES

Oxide	Melting point [°K]	Boiling point [°K]	Heat of formation [Kcal/mole O_2]
BeO	2 850	4 200	270
CeO_2	2 900	-----	233
Cr_2O_3	2 700	4 300	180
HfO_2	3 100	5 400	271
MgO	3 100	4 000	292
ThO_2	3 350	4 700	293
ZrO_2	3 000	5 300	260

From Table 2, the best material appears to be HfO_2. However, pure hafnia is a very rare and expensive material. The second best-ranking combinations are ThO_2 and ZrO_2. These oxides are easily available and have therefore been selected for the samples.

3.2 POROSITY

There are various reasons to choose samples with as large a porosity and pore size as possible:

1) The effusion rate through the sample increases with the porosity and with the pore diameter, as has been discussed in 1.2.

2) In the course of preliminary laser heating experiments, we have found out that the resistance to thermal shock increases markedly with the porosity.

The maximum porosity and pore diameter respectively are limited by the mechanical stability of the material and by the mean free path of the molecules to be separated. If the pore diameter exceeds the mean free path, the effusion flow regime will gradually loose its mass-selective properties.

The experiment has been carried out at a total upstream pressure of the order of 0.15 Torr, with a possibility for extension up to a few Torr (see section 1.3). The corresponding mean free path can be expressed as [22]:

Gas	7.60 Torr 600°K	7.60 Torr 3000°K	0.15 Torr 600°K	0.15 Torr 3000°K
Air (or H_2O)	12.10^{-3} mm	0.06 mm	0.6 mm	3 mm
Hydrogen	24.10^{-3} mm	0.12 mm	1.2 mm	6 mm

The grain size for the preparation of the samples has been set at 1 mm, which corresponds to an average pore diameter of about 0.1 mm.

In the region of the hot spot, this value is sufficiently low to permit an extension of the reaction pressure up to a few Torr without losing the mass-selective properties. It is also sufficiently high to still allow for a significant flow rate at 0.15 Torr.

In the cooler region near the rim of the disc sample, where leakage occurs between the disc and the supporting tube, the mean free path is reduced but

remains still in the mm range if P = 0.15 torr and T > 600°K. Thus the leakage flow should also be mass-selective, and should contribute to hydrogen and oxygen separation. However, an extension to a few Torr would require in this case the sample to be sealed to the tube or at least the width of the leakage channels to be reduced down to 0.02 mm.

3.3 PREPARATION PROCEDURE

The samples have been made from powder of ThO_2 puriss. from Fluka AG and ZrO_2 (HfO_2) 99.6% from Ugine Kuhlmann. The grain size of these powders is in the micron range. The preparation itself includes two sintering cycles.

In the first cycle, the powder is mixed with an organic binder (camphor) and cold-pressed (room temperature, 5 000 kg/cm^2) in the form of compact pellets of 25 mm diameter and 4 mm thickness. The binder is necessary to impart the pellets with enough mechanical strengtn to withstand the extraction from the press and the transportation to the vacuum furnace without damage.

The pressed pellets are placed in a tungsten crucible surrounded by a tantalum resistive heater and gradually heated under vacuum. When all the camphor has been evaporated, the temperature is further increased and held for 5 to 10 hours at 1 800°C to 1 900°C. After cooling down, the pellets are crushed and sieved to collect ThO_2 or ZrO_2 grains in the 1 mm size range.

In the second sintering cycle, the selected grains are again mixed with the organic binder and cold-pressed. The same press moulds are used to produce discs of 25 mm diameter and 4 mm thickness, but cold pressing is carried out at a reduced pressure (1 000 kg/cm^2) in order not to compact the grains too much.

The same high temperature vacuum sintering procedure as described for the first cycle is then reproduced. The resulting sintered discs present an overall porosity of the order of 35% with many macropores in the size range of 100 µ.

Fig. 5a represents two typical ZrO_2 discs. The left sample is as sintered. Its appearance is dark grey. The right sample has been submitted to laser heating in air and water vapor. All the heated parts present the typical white color of fully oxidized ceramics. According to Toropov et al. [20], the composition of the dark region is $ZrO_{1.97}$, owing to some oxygen loss during the vacuum treatment.

Fig. 5b shows three ThO_2 samples. To the left, a sample with small grain size is displaid; it has been produced by means of only one sintering cycle and has been submitted to 120 W laser heating in air. This sample has been prepared by means of a smaller press mould and is thus only 20 mm in diameter and 2 mm thick. The central item is a larger sample (25 mm x 4 mm) ready for crushing. To the right, a ThO_2 sample after the second sintering cycle is shown. It is to be noted that the sintered ThO_2 samples appear less dark than the ZrO_2 samples, probably indicating less oxygen loss.

4. CALIBRATION PROCEDURES

4.1 MEASUREMENT OF THE SAMPLE TEMPERATURE

Accurate pyrometric measurement of the temperature of a strongly selctive emitting material like ThO_2 or ZrO_2 is a delicate problem which has been left aside in the present phase work.

The temperature of the hot spot has been estimated from the measured laser power and the total thermal emissivity ε of the oxide.

The surface temperature, as determined by the radiant balance, can be expressed as:

$$T = \sqrt[4]{P / \varepsilon\sigma S} \qquad (4)$$

where P is the beam power, in W,
$\sigma = 5.7 \cdot 10^{-8}$ W.m^{-2} (°K)$^{-4}$
S is the area of the hot spot taken as 5.10^{-5} m^2

For ZrO_2, the emissivity ε lies between 0.5 and 0.9 [23] above 2 000°K. Taking an average value of $\varepsilon = 0.7$, we find:

for P = 20 W, T = 1 780°K
60 W 2 340°K
100 W 2 660°K

4.2 PARTIAL PRESSURE MEASUREMENTS

The relative sensitivity S of the quadrupole mass spectrometer at any given mass number can be expressed by the usual relationship:

$$i_{output} = S \cdot p \qquad (5)$$

where: $i_{output\ multiplier}$ is the output current measured at the collector of the electron multiplier

i^- is the ionizing electron current (here taken as the total cathode emission)

p is the partial pressure of a given mass species.

The knowledge of S allows for the determination of the partial pressures from the measured output current of the spectrometer at the corresponding mass in the spectrum.

Since S depends on the gain of the electron multiplier which varies slowly as a function of the time, owing to changes in the surface state of the dynodes, generally only the relative values of S for the various masses to be monitored are determined. The absolute value of S can be estimated for each experimental run by comparison of the spectrometer output with the indication of a total pressure gauge (BAG gauge) for a well-known and relatively inactive gas like N_2.

In the present work, the more important masses to be monitored are:

H_2 (M = 2); H_2O (M = 18); N_2 (M = 28); O_2 (M = 32).

Values of S for the QUAD spectrometer used in this work have been experimentally determined by Petermann [24] as:

$$S_{H_2} = 6 \text{ to } 10 \cdot 10^4 \text{ Torr}^{-1}$$

$$S_{N_2} = 6 \text{ to } 9 \cdot 10^4 \text{ Torr}^{-1}.$$

These values result from many runs and can be considered as well established. $S_{H_2}/S_{N_2} \sim 1$ can thus be used.

The relative sensitivity for O_2 with respect to N_2 has been determined by introducing atmospheric air (80% N_2/20% O_2) through the microleak into the QUAD and recording the relative readings at various pressure levels. This is summarized in Table 3.

TABLE 3 - DETERMINATION OF THE RELATIVE SENSITIVITY FOR O_2

Total pressure BAG gauge [Torr]	QUAD reading at mass 28 [mV]	QUAD reading at mass 32 [mV]	S_{O_2} / S_{N_2}
$3 . 10^{-8}$	30	1	0.05
$3 . 10^{-7}$	1 800	14	0.03
$1.8 . 10^{-6}$	12 000	80	0.025
$8.2 . 10^{-6}$	48 000	360	0.03

The higher value for S_{O_2} / S_{N_2} obtained at 3.10^{-8} Torr is probably due to residual O_2 in the vacuum system from O_2 previously introduced at higher pressure. It can thus be concluded that $S_{O_2} / S_{N_2} \sim 0.03$.

H_2O is a condensable gas and substantial physical adsorption on the walls render the calibration of this gas difficult. It also depends on the adjustment of the QUAD microleak.

To minimize the influence of such effects, H_2O has been tentatively calibrated from various N_2/H_2O mixtures introduced from the reactor into the QUAD section under the same conditions as during experiment. One can write:

$$\frac{P_1}{P_2} = \frac{P^1_{H_2O} + P^1_{N_2}}{P^2_{H_2O} + P^2_{N_2}} = \frac{r^1_{H_2O}/S_{H_2O} + r^1_{N_2}/S_{N_2}}{r^2_{H_2O}/S_{H_2O} + r^2_{N_2}/S_{N_2}} \quad (6)$$

where: p_1 and p_2 are the total vessel pressures, for mixtures 1 and 2;

$p^1_{H_2O}$ and $p^2_{H_2O}$ are the partial pressures for H_2O, for mixtures 1 and 2;

$p^1_{N_2}$ and $p^2_{N_2}$ are the partial pressures for N_2 for mixtures 1 and 2;

$r^1_{H_2O}$ and $r^2_{H_2O}$ are the QUAD readings, in mV, H_2O for mixtures 1 and 2;

$r^1_{N_2}$ and $r^2_{N_2}$ are the QUAD readings, in mV N_2 for mixtures 1 and 2;
S_{H_2O} and S_{N_2} are the QUAD sensitivities, resp. for H_2O and N_2.

From (6) the following expression is derived:

$$\frac{S_{H_2O}}{S_{N_2}} = \frac{p_2 r^1_{H_2O} - p_1 r^2_{H_2O}}{p_1 r^2_{N_2} - p_2 r^1_{N_2}} \qquad (7)$$

Tables 5 and 6 give the corresponding values for mixture 1 (event 3) and mixture 2 (event 4):

$p_1 = 27 \cdot 10^{-3}$ Torr $\qquad p_2 = 150 \cdot 10^{-3}$ Torr

$r^1_{H_2O} = 3.5$ mV $\qquad r^2_{H_2O} = 105$ mV

$r^1_{N_2} = 83.5$ mV $\qquad r^2_{N_2} = 79.5$ mV

Whence, for the water vapor relative sensitivity: $S_{H_2O} / S_{N_2} \sim 0.2$.

To convert the QUAD readings (in mV) into partial pressure values (in Torr) the conversion factor for N_2 must first be determined. From Table 3, follows on the average:

$$\frac{P_{N_2}}{r_{N_2}} \approx \frac{0.8\ P_{BAG}}{r_{N_2}} \approx 1.3 \cdot 10^{-10}\ \frac{\text{Torr}}{\text{mV}}$$

Now, the conversion factor for H_2, O_2 and H_2O can be estimated as the ratio between the conversion factor for N_2 and the relative sensitivity for the gas considered as referred to N_2.

These various sensitivities and conversion factors are summarized in Table 4.

TABLE 4 - RELATIVE QUAD SENSITIVITIES AND CONVERSION FACTORS

Gas	H_2	H_2O	N_2	O_2
Mass	2	18	28	32
Relative sensitivity	1	0.2	1	0.03
Conversion factor [10^{-10} Torr/mV]	1.3	6.5	1.3	43

Remark

Owing to the nature of the spectrometer measurements which depend on the conductance of the microleak connecting the reactor compartments to the QUAD system, on the pumping rate of the various gases within the QUAD system, and on the performance of the QUAD itself, the determination of the conversion factors gives only an approximation.

It will be shown in the discussion of the experiments that, in fact, the essential results (dissociation degree and separation performance) can be derived independently and do not depend on the calibration of the partial pressures. However, a knowledge of the partial pressures is useful to compare the respective concentrations of the reaction gases.

5. REACTOR OPERATION

5.1 INTRODUCTION

Once the functioning of the system had been tested and the control parameters adjusted, a detailed operational procedure was progressively set-up. This procedure, which will be described below, was repeated four times.

Runs one and two were performed with a first ZrO_2 disc sample, similar to the sample shown in Fig. 5a. Runs three and four were carried out with the ZrO_2 sample shown in Fig. 5a. The same qualitative results have been observed during operation of the reactor from run one to run four.

Run four was carried out very carefully and completely monitored. The run was decomposed into 32 events and for each event a photograph of the QUAD spectrum was taken. Table 5 represents the sequence of events and Table 6 gives the QUAD reading for each mass and for each event.

TABLE 5 - SEQUENCE OF EVENTS DURING RUN FOUR

Event			Pirani readings		H_2O micro-leak	Laser beam power (W)
No.	Time (min)	Description QUAD connection	Upstream (μ Hg)	Downstream (μ Hg)		
2	0	residual QUAD atmosphere	-	-	-	-
3	15	upstream	27	25	OFF	-
4	47	upstream	150	70	ON	-
5	50	downstream	160	74	ON	-
6	54	downstream	25	25	OFF	-
7	57	downstream	25	25	OFF	-
8	60	downstream QUAD microleak slightly closed	25	25	OFF	-
9	68	downstream	29	26	OFF	19
10	70	downstream	29	26	OFF	65
11	71	downstream	25	22	OFF	97
12	73	downstream	23	22	OFF	19
13	80	downstream	150	65	ON	19
14	81	downstream	180	75	ON	65
15	83	downstream	180	75	ON	97
16	85	downstream	160	62	ON	19
17	95	upstream	29	25	OFF	19
18	97	upstream	30	23	OFF	65
19	99	upstream	29	22	OFF	97
20	102	upstream	23	22	OFF	19
21	105	upstream	155	65	ON	19
22	106	upstream	180	72	ON	52
23	108	upstream	190	75	ON	91
24	113	upstream	160	66	ON	-
26	124	upstream	22	28	OFF	-
27	128	upstream	28	25	OFF	-
28	130	upstream	145	66	ON	-

TABLE 6 - QUAD READINGS* FOR EACH PEAK OF EACH EVENT DURING RUN FOUR

Mass / Event	2 H_2	3 HD	14 (N_2)	15 (CH_4)	16 CH_4 (O_2)	17 (H_2O)	18 H_2O	19 ?	26 (C_2H_6)	27	28 N_2 CO C_2H_6	29 C_3H_8 (C_2H_6)	30	32 O_2	39 C_3H_3	40 Ar	41 (C_3H_5)	42 (C_3H_6)	44 CO_2 (C_3H_8)
2	5.5	0.5	-	0.5	4.5	1	0.5	1	-	-	1.5	-	-	1	-	-	-	-	0.5
3	5	0.5	14	0.5	3.5	2	3.5	1	-	-	83.5	1	-	1.5	-	3.5	-	-	0.5
4	17.5	3.5	2	1	9	28.5	105	1	-	0.5	19.5	0.5	-	14	-	-	-	-	4.5
5	17.5	3.5	2	1	7.5	22	74.5	1	-	0.5	14	0.5	0.5	15	0.5	-	-	-	3.5
6	14	2.5	11	1.5	5	10	36	0.5	-	0.5	90	0.5	-	9	0.5	2	-	-	2.5
7	13	2	15.5	1	4.5	8.5	28.5	0.5	-	0,5	118.5	1	-	7.5	0.5	2	-	-	2.5
8	9	2	11.5	0.5	3.5	5.5	19.5	0.5	-	-	87.5	1	-	4.5	-	2	-	-	2.5
9	13	2	13	6.5	9	4.5	14	-	4.5	6.5	96.5	6.5	4.5	3.5	1	2.5	1.5	0.5	3.5
10	48	2	12	12	15.5	4.5	14	-	3.5	5.5	76.5	5.5	3.5	2	1	2	1	0.5	3.5
11	42.5	2	11.5	6.5	10	4.5	12	-	1.5	2	70	2	1.5	3	0.5	2	0.5	0.5	4.5
12	18.5	2	17.5	10	13	4.5	11	-	3.5	6	114	6	3.5	2	1.5	3.5	1.5	1	3.5
13	17.5	2	2	2	4.5	7	21	-	0.5	1	16	1	0.5	3	-	1	-	-	3.5
14	96.5	2	1	2	6.5	8.5	24	-	0.5	0.5	13	0.5	0.5	5.5	-	-	-	-	5
15	120	2	1.5	2	6.5	7.5	24	-	-	0.5	13	0.5	-	7.5	-	-	-	-	5.5
16	20	2	1	1.5	5.5	9	28.5	-	-	0.5	10.5	0.5	-	5.5	-	-	-	-	4
17	18.5	3	7.5	4	7	7	20	-	1.5	2	48.5	2	1.5	5.5	0.5	2	0.5	-	3
18	54.5	3.5	7	6.5	11.5	5.5	17.5	-	1.5	2	44	2	1.5	4	-	1.5	-	-	5
19	48	3.5	5.5	4.5	8	5.5	16	-	1	1.5	42.5	1.5	1	4	-	1.5	-	-	6.5
20	18.5	3.5	11	8.5	12.5	5.5	14	-	2.5	4.5	69	4.5	2.5	3	0.5	2	-	-	4
21	31	4.5	2	3.5	9	19	62	1	1	2	16	2	1	13	-	-	-	-	5
22	112	4	2	4	11.5	19.5	67	1	1	1.5	16	1.5	1	15	-	-	-	-	9
23	197	4.5	2	4.5	11.5	19.5	67.5	0.5	0.5	1	14	1	0.5	25	-	-	-	-	9.5
24	30	5.5	1.5	3	11	28	98	1	-	0.5	11	0.5	-	19	-	-	-	-	3.5
26	32.5	6	4	3.5	10	16	54	0.5	1	1.5	30.5	2	1	13	-	1.5	-	-	3
27	25	6	6.5	3.5	7.5	11.5	35	0.5	1	1.5	46	2	1	9.5	-	2	-	-	3.5
28	26.5	6.5	3	3.5	11	22	74	1	0.5	1.5	19	2	1	15	-	0.5	-	-	3.5

* The QUAD readings are given in mV, corresponding to the voltage recorded at the output of the electron multiplier operated at 2 500 V. Emission current was 0.4 mA, and electron energy 80 eV. The output of the electron multiplier was connected to a 1 MΩ oscilloscope input.

5.2 DETAILED TESTING PROCEDURE

Before each run, the QUAD is operated on its own residual atmosphere ($< 10^{-8}$ Torr) for one hour to achieve complete stabilization. During this time, the laser is warmed up with the chopper adjusted to a position which reflects completely the beam onto the brick arrester. From time to time the power of the beam is controlled with the laser probe. After twenty minutes, the laser is adjusted for maximum power (by observing the hot spot on the brick wall). Both compartments of the vacuum vessel (upstream and downstream) are pumped-down to their residual pressure (of the order of 2.10^{-2} Torr). The H_2O microleak is heated to about 40°C to avoid water condensation and cold water is circulated around the vacuum vessel. The reactor is thus ready to be operated.

The upstream valve is opened and the QUAD microleak carefully opened until the total pressure in the QUAD section has increased by a factor of about 10 (event 3). The QUAD now displays the residual atmosphere of the vacuum vessel (upstream compartment). As can be seen in Fig. 6a, this atmosphere consists essentially of N_2 (masses 28 and 14) and in traces of H_2 (mass 2), CH_4 (mass 16), H_2O (masses 17 and 18), O_2 (mass 32), Ar (mass 40) and CO_2 (mass 44).

Water vapor is introduced by opening the H_2O microleak until the upstream total pressure rises from 27 μ Hg to 150 μ Hg and up (event 4). The new composition of the upstream atmosphere is shown in Fig. 6b. A strong build-up of the H_2O peaks is observed, together with a progressive disappearance of the N_2 peaks. This can be explained by diffusion pumping of residual N_2 by the water vapor streaming from the vessel to the pumps.

The QUAD is connected downstream. This operation is carried out (without changing the adjustment of the QUAD microleak) by closing the upstream valve and opening the downstream valve. The composition of the downstream atmosphere is verified (event 5). Despite further increase of the total pressure (from 150 to 160 μ Hg) within the upstream vacuum section, the H_2O peak is noted at 74.5 mV and going down instead of 105 mV and going up. This shows

that the difference in the total pressure between the upstream and the downstream sections during the upstream and the downstream sections during water vapor introduction is reflected by the H_2O readings of the QUAD, if one takes into account a time-lag due to wall adsorption of H_2O.

To test the time-lag, the H_2O microleak is closed and the delay of the H_2O peak is observed (events 6-7). This question of time-lag will be discussed later on. It can be noted that, as soon as the microkeak is closed, the N_2 peak reappears because there is no more diffusion pumping by the H_2O stream.

The QUAD microleak is slightly closed (ultimate adjustment). The time-lag of the H_2O response is again observed (events 8 to 9).

During the introduction of H_2O, a marked rise in the oxygen peak is detected (see mass 32, Fig. 6b). It is thought that this peak originates from oxygen dissolved in the water introduced.

The residual reaction of the system to laser heating in the absence of water introduction is tested for the downstream section (events 9-12). To do this, the chopper is gradually adjusted at 15%, 50%, 75% and again at 15% of the power for a free passage of the laser beam. As the measured total beam power is 130 W, this corresponds to 19, 65, 97 and 19 W. A slight increase in the partial pressures of H_2 and O_2 is noted, which is attributed to the dissociation of water adsorbed within the porous ceramic dis.

Water vapor is reintroduced within the reactor and the laser heating cycle is reproduced (events 13 to 16). A marked increase in the H_2 and O_2 partial pressures is observed owing to the dissociation of flowing H_2O by the hot spot on the disc. The respective heights of the H_2 peak are shown in Fig. 7a (laser power 97 W) and 7b (laser power 19 W). The variations of the O_2 peak are not easily observed in the pictures because of the low sensitivity for O_2. They can be monitored with better accuracy by changing the oscilloscope vertical scale.

The QUAD is then connected upstream, without changing the adjustment of the QUAD microleak, by closing the downstream valve and opening the upstream valve.

The laser heating and water introduction sequence of events 9 to 16 is then reproduced in order to observe the residual reactions of the system to laser heating when H_2O is not introduced (events 17 to 20), and to observe the dissociation of the flowing water vapor when water is again introduced (events 21 to 24) for the upstream section. The resulting evolution of the H_2 peak is shown in Fig. 8a (laser power 91 W) and 8b (laser power off).

Before shutting down the reactor, the H_2O microleak is once again closed and reopened (events 26 to 28) in order to test the evolution of the various peaks after operation of the reactor.

6. DISCUSSION OF THE PERFORMANCE

6.1 PRESENTATION OF THE RESULTS

The values of the partial pressures for the main QUAD peaks (H_2, H_2O, N_2 and O_2) during run four (events 4 to 28) have been calculated from Table 6, using the conversion factors of Table 4.

The evolution of these partial pressures is summarized in Fig. 9. The total pressures recorded in the upstream and downstream sections are also represented. The events are marked on a time scale (x-axis). The sequence of laser heating is shown in the upper part of the figure together with the sequence of water introduction.

The evolution of the H_2O and the O_2 partial pressures for the first events on the left of Fig. 9 (events 5 to 9) shows the time-lags already mentioned in section 5.2. Associated with these time-lags, background pressures for both H_2O and O_2 can be observed when the H_2O microleak is switched off. These background pressures have been denoted as "QUAD background pressures" in Fig. 9. Another background pressure is noted in Fig. 9 for O_2 corresponding to the level of dissolved oxygen introduced together with the water vapor. This background pressure of dissolved O_2 is useful to appreciate the amount of oxygen originating from dissociated H_2O.

Fig. 9 allows for a direct comparison between the upstream and downstream results. It can be seen, for instance, that the small rises in the H_2 and O_2 pressure, during laser heating and in the absence of the H_2O flow, are of the same magnitude, independent of the compartment monitored. This can be explained by dissociation of water vapor adsorbed within the porous disc. The small amplitude corresponds to the limited amount of adsorbed water available while the absence of selectivity is due to the fact that the desorbed gases diffuse indifferently upstream and downstream from within the ceramic disc.

The situation is quite different when the porous disc is heated in the presence of a water vapor flow.

A first observation concerns the general level of the upstream partial pressures which is about three times the level of the downstream pressures. This is in agreement with the variations of the total pressures directly monitored within the reactor (from 25 to 180 μ Hg giving a variation of 155 μ Hg which is to compare with 75-25 = 50 μ Hg).

It can be observed that the H_2O partial pressure rises continuously from the introduction of the water vapor flow (event 12 and event 20) with a marked step (event 15 and event 23) up to the end of each introduction cycle (event 16 and event 24). The step corresponds to the moment of maximum laser heating. The difference between the step and a smooth extension of the H_2O curve represents the missing amount of dissociated H_2O. The portions of the curves corresponding to this difference have been shaded.

The O_2 partial pressure also rises continuously from event 12 and 20 respectively up to event 16 and 24 (background of oxygen dissolved in the water), with a marked peak (events 15 and 23) corresponding to the maximum laser heating. The difference between the peaks and the background has also been shaded. It represents the amount of oxygen originated from dissociated water vapor.

The H_2 partial pressure curves are more simple, as they have almost no background. Marked peaks are again observed for events 15 and 23 (maximum laser heating) corresponding to a production of hydrogen from dissociated H_2O.

Considering the shaded areas in Fig. 9, one can see that the amount of hydrogen is larger than the amount of oxygen in the downstream section (event 15) while the situation is reversed in the upstream section (event 23). This shows that the dissociation products (oxygen and hydrogen) are separated selectively; more hydrogen is flowing from the upstream to the downstream section than oxygen.

6.2 FRACTION OF DECOMPOSED H_2O

As discussed before, the amount of dissociated water vapor is represented by the difference of H_2O partial pressure between the step following event 15 (downstream) or event 23 (upstream) and the full value following event 16 (downstream) or event 24 (upstream).

These differences are respectively (see Fig. 9):

- Downstream: 185.10^{-10} Torr - 156.10^{-10} Torr = 29.10^{-10} Torr

- Upstream: 637.10^{-10} Torr - 439.10^{-10} Torr = 198.10^{-10} Torr.

To obtain the dissociation degree, these values must be compared to the reference H_2O values of event 16 or 24, corrected for the background owing to the time-lay within the QUAD section. From Fig.9, those backgrounds can be estimated at 50.10^{-10} Torr (event 16) and 65.10^{-10} Torr (event 24) respectively. The corrected reference values are therefore

- Dowstream: 185.10^{-10} Torr - 50.10^{-10} Torr = 135.10^{-10} Torr

- Upstream: 637.10^{-10} Torr - 65.10^{-10} Torr = 572.10^{-10} Torr.

The observed dissociation degrees appear then to be:

- Downstream = $\alpha = 29.10^{-10}$ Torr / 135.10^{-10} Torr = 0.21

- Upstream = $\alpha = 198.10^{-10}$ Torr / 572.10^{-10} Torr = 0.35.

Remark

The determination of the dissociation degree is not affected by calibration factors, since the derivation involves only values of H_2O partial pressures. It can, howver, be affected by variations of the conductance between the upstream and the downstream sections as a function of the temperature of the disc.

Normally, the conductance is expected to decrease when the temperature is increased, as $\sqrt{T}$. However, owing to thermal expansion effects, the conductance can also be increased (opening of small cracks or augmented lateral leakage between the disc and the supporting tube). Anyhow, the effect of an increase of conductance would be to increase the apparent upstream dissociation degree α and to decrease the apparent downstream α, while the effect of a decrease of conductance would be to increase the apparent downstream α and to decrease the apparent upstream α. From the numerically determined values of α, it appears that the thermal expansion effects have been more substantial leading thus to a higher apparent upstream α (0.35) than the apparent downstream value (0.21). The real α value must lie between these two values. Finally:

$0.21 < \alpha < 0.35$, or $\alpha \sim 30\%$.

The comparison between this experimental value and the theoretical curves for the dissociation degree has been discussed in section 1.3 (see Fig. 1).

The amount of dissociated H_2O can also be compared to the amount of produced H_2 and O_2. Fig. 9 shows that these values (shaded acreas for events 15 and 23) are of the same magnitude. Because of the uncertainties in the calibration of the partial pressures, it is difficult to give any more precise indication.

6.3 SEPARATION PERFORMANCE

In this section, the relative experimental conductances between the upstream and the downstream compartments are determined for the various reacting gases (H_2, H_2O and O_2); they are compared to the theoretical values expected for a Knudsen flow regime through the porous wall.

6.3.1 THEORETICAL RELATIVE CONDUCTANCES

The two compartments (upstream and downstream) separated by the porous disc of conductance U, are considered for a given species of molecular mass M. U is defined as:

$$U = P \frac{dV}{dt} / \Delta P \qquad (8)$$

Where P is the partial pressure flowing at a volumic rate dV/dt through a pressure gradient ΔP.

It has been seen (Section 1.2) that Knudsen's law for the molecular flow regime can be expressed as:

$$\frac{dn}{dt} \sim P \frac{dV}{dt} = U_o \cdot \Delta P / \sqrt{M} \qquad (9)$$

where U_o is a factor depending only on the geometry and the absolute temperature T. A correction due to the "slip" effect (sticking coefficient < 1) is hereby not taken into consideration.

From the definition of the conductance U and the law of Knudsen, it is derived:

$$U = U_o / \sqrt{M} \qquad (10)$$

The theoretical relative conductances for the gases considered can thus be expressed as:

$$U_{H_2} / U_{O_2} = \sqrt{M_{O_2}/M_{H_2}} = \sqrt{32/2} = 4.00$$

$$U_{H_2O} / U_{O_2} = \sqrt{M_{O_2}/M_{H_2O}} = \sqrt{32/18} = 1.33$$

6.3.2 EXPERIMENTAL RELATIVE CONDUCTANCES

Let P_i^u be the upstream partial pressure for the species i, and
P_i^d be the downstream partial pressure for the same species i.

From the definition of U in section 6.3.1, it follows:

$$U_i = P_i \frac{dV}{dt} / \Delta P_i = P_i \frac{dV}{dt} / (P_i^u - P_i^d) \qquad (11)$$

Now, the downstream compartment is pumped by a volumetric (sliding vane) pump characterised by a pumping power $U_{pump} = dV/dt$ which is independent of the gas species in the pressure range considered.

Thus:

$$U_i = U_{pump}\, P_i^d / (P_i^u - P_i^d) \qquad (12)$$

The relative conductance for two gas species i and j is finally given by:

$$U_i/U_j = \frac{P_i^d\,(P_j^u - P_j^d)}{P_j^d\,(P_i^u - P_i^d)} \qquad (13)$$

Remark

The expression for U_i is independent of the partial pressure calibration factor, since U_i is the ratio of two partial pressures for the same species i.

Fig. 9 gives the upstream partial pressures to be considered (event 23) and the corresponding downstream partial pressures (event 15). After subtraction of the estimated QUAD background values, it follows:

From event 15:

$P^d_{H_2} = 156.10^{-10} - 25.10^{-10} = 131.10^{-10}$ Torr

$P^d_{H_2O} = 156.10^{-10} - 50.10^{-10} = 106.10^{-10}$ Torr

$P^d_{O_2} = 323.10^{-10} - 90.10^{-10} = 233.10^{-10}$ Torr.

From event 23:

$P^u_{H_2} = 256.10^{-10} - 40.10^{-10} = 216.10^{-10}$ Torr

$P^u_{H_2O} = 439.10^{-10} - 65.10^{-10} = 374.10^{-10}$ Torr

$P^u_{O_2} = 1080.10^{-10} - 100.10^{-10} = 980.10^{-10}$ Torr.

Thus finally:

$$U_{H_2}/U_{O_2} = \frac{131 \times (980-233)}{233 \times (216-131)} = 4.94$$

$$U_{H_2O}/U_{O_2} = \frac{106 \times (980-233)}{233 \times (374-106)} = 1.27$$

The values for the partial pressure of oxygen have been taken for the total O_2 component, i.e. without making any distinction between O_2 originally dissolved in the water and O_2 from the dissociated water vapor flow.

To test the consistency of the results, the following distinction can now be made. From Fig. 9, the background of dissolved O_2 is estimated at:

$p^u_{O_2}$ dissolved = 580.10^{-10} Torr (event 23)

$p^d_{O_2}$ dissolved = 210.10^{-10} Torr (event 15).

The partial pressures of O_2 from dissociated H_2O can thus be calculated for these events as:

$p^u_{O_2}$ dissociated = $(1080.10^{-10} - 580.10^{-10}) = 500.10^{-10}$ Torr (event 23)

$p^d_{O_2}$ dissociated = $(323.10^{-10} - 210.10^{-10}) = 113.10^{-10}$ Torr (event 15).

Thus:

$$\frac{U_{O_2}\ (\text{dissociation})}{U_{O_2}\ (\text{dissociation + dissolution})} = \frac{113 \times (980-233)}{233 \times (500-113)} = 0.94$$

6.3.2 - COMPARISON OF THE THEORETICAL AND THE EXPERIMENTAL CONDUCTANCES

The relevant values are summarized in Table 7.

TABLE 7 - COMPARISON OF THEORETICAL AND EXPERIMENTAL CONDUCTANCES

	U_{H_2} / U_{O_2}	U_{H_2O} / U_{O_2}	$U_{O_2}(diss.)/U_{O_2}(tot.)$
Theoretical (Knudsen)	4.00	1.33	1.00
Experimental	4.94	1.27	0.94

From Table 7, it can be concluded that, within the margin of experimental error, the conductances determined for the various reacting gases obey the laws of Knudsen flow. The separation performance between hydrogen and oxygen appears even higher than theoretically predicted.

7. CONCLUSIONS AND RECOMMENDATIONS

The present conceptual study indicates that an industrial reactor for the production of hydrogen by direct thermal water splitting would have an overall useful yield of 40% with cooling requirements as low as 25%. This presupposes that water vapor can be dissociated at 2500°K under a total pressure of 0.1 atm with a dissociation degree of 10%, and that the reaction products can be flowed at high temperature through a porous membrane under a Knudsen effusion regime.

A first experimental demonstration of direct water splitting has been successfully carried out in the present work. Water vapor has been dissociated with a dissociation degree of the order of 30% at 2600°K under a total pressure of 0.18 Torr. It has been shown that this achievement is compatible with the theoretical requirements: hydrogen and oxygen from the dissociation reaction have been separated through a ZrO_2 porous membrane in the proportions of a Knudsen effusion regime.

Owing to time and budget limitations it has not been possible during the present work to operate the experimental reactor at the total pressure of 0.1 atm. In fact, as explained in Chapter 1.3, operation at higher pressures would have required to thermostatise the entire reactor in order to avoid water vapor condensation.

It is recommended that the experimentation undertaken during the present work be continued and expanded in order to operate the reactor at various total pressures, up to a few Torrs in a first stage, and up to 0.1 atm in a second stage.

ThO_2 should be tested as an alternative material for the selective membrane.

The calibration procedures should be improved.

It is also recommended that the planning of a four-year development program be established in detail, with the objective of realizing an experimental 15 kW-solar direct water splitting reactor.

If a proper effort is made, the first industrial realizations for hydrogen production in the lands situated between 20° and 40° latitude could expected to be initiated towards 1990.

Spatial applications can be envisaged for the year 2000.

ACKNOWLEDGEMENT

It is a pleasure for the author to thank Dr. J. KELLEY, Hydrogen Systems and Technology Manager and Dr. D. LAWSON, Program Manager both from the Jet Propulsion Laboratories, Pasadena, for their valuable advice and constant active support of the project.

The author's thanks go also to Dr. K. BECCU, Program Director and to Dr. D. GROSS, Group Leader and Co-inventor of the new water splitting concept, both from Battelle-Geneva, for their many fruitful discussions and careful proof-reading of the manuscript.

8. REFERENCES

[1] An analysis of hydrogen production via closed-cycles schemes
R.E. Chao and K.E. Cox
THEME Conference Miami Beach Florida (1974) paper S13

[2] Caractéristiques et performances énergétiques du four solaire de 1000 kW du CNRS
F. Trombe, A. le Phat Vinh
C.R. Acad. Sci. Paris 272 (1971) p. 1104

[3] Properties of ordinary water-substance
N.E. Dorsey
Reinhold Publishing Corp. (1940)

[4] Hydrogen and oxygen from water
E.A. Fletcher and R.L. Moen
Science 197 (1977) p. 1050

[5] Hydrogen production from water utilizing solar heat at high temperatures
T. Nakamura
Solar Energy 19 (1977) p. 467

[6] Pompes et groupes de pompage Roots
P31-197106f, Balzers AG

[7] Thoria effusion membranes
R.B. Diver and E.A. Fletcher
Ceramic Bulletin 56 (1977) p. 1019

[8] Feasibility of hydrogen production by direct water splitting at high temperature
S. Ihara
Int. J. Hydrogen Energy 3 (1978) p. 287

[9] Dispositif générateur d'hydrogène
J. Fally/C.G.E.
Brevet d'invention belge No 845009 (1977)

[10] Materials and techniques for electron tubes
W.H. Kohl
Reinhold Publishing Corp. (1960) p. 618

[11] Diffusion in and through solids
R.M. Barrer
Cambridge University Press (1951)

[12] Solar reactor for hydrogen production by direct thermal splitting of water inside a porous wall
Technical Note, Battelle-Geneva Research Centers (1975)

[13] Ceramic microstructures
R.M. Fulrath, J.A. Pask
Proc. Third Int. Materials Symp., University of California (1966)

[14] Water vapor pressure tables
Handbook of chemistry and physics
CRC Press (1975) Section D-181

[15] Oriel infrared devices (1978) p. 6, Darmstadt, Germany

[16] Heliostat manufacturing technology
K. Drumkeller
Large solar central systems, semi-annual review, Dallas (1978)

[17] Solar power via satellite
P.E. Glaser
IEEE Intercon Techn. Papers (1973) Session 6

[18] The colonization of space
G.K. O'Neill
Physics Today 27 (1974) p. 32

[19] Refractory materials
Handbook of chemistry and physics, Section D-51

[20] High temperature chemistry of silicates and other oxide systems
N.A. Toropov and V.P. Barzakovskii
CIB Consultants, Plenum Publish Corp N.Y. (1966)

[21] The thermochemistry of chemical substances
F.R. Bichowsky and F.D. Rossini
Reinhold Publishing Corp. (1936)

[22] An introduction to the kinetic theory of gases
Sir J. Jeans
Cambridge (1960) p. 48

[23] Thermophysical properties of high temperature solid materials
S.X. Tonloukian
Vol. 4, part I = Simple oxygen compounds and their mixtures
McMillan (1967) p. 589

[24] Comparison between a quadrupole mass filter and a omegatron mass spectrometer under low pressure conditions
L.A. Petermann
Ergebnisse Europäischer Ultrahochvakuum-Forschung (1968) p. 113
Leybold Heraeus Germany

Geneva, May 1980
193-4811/PG/mf

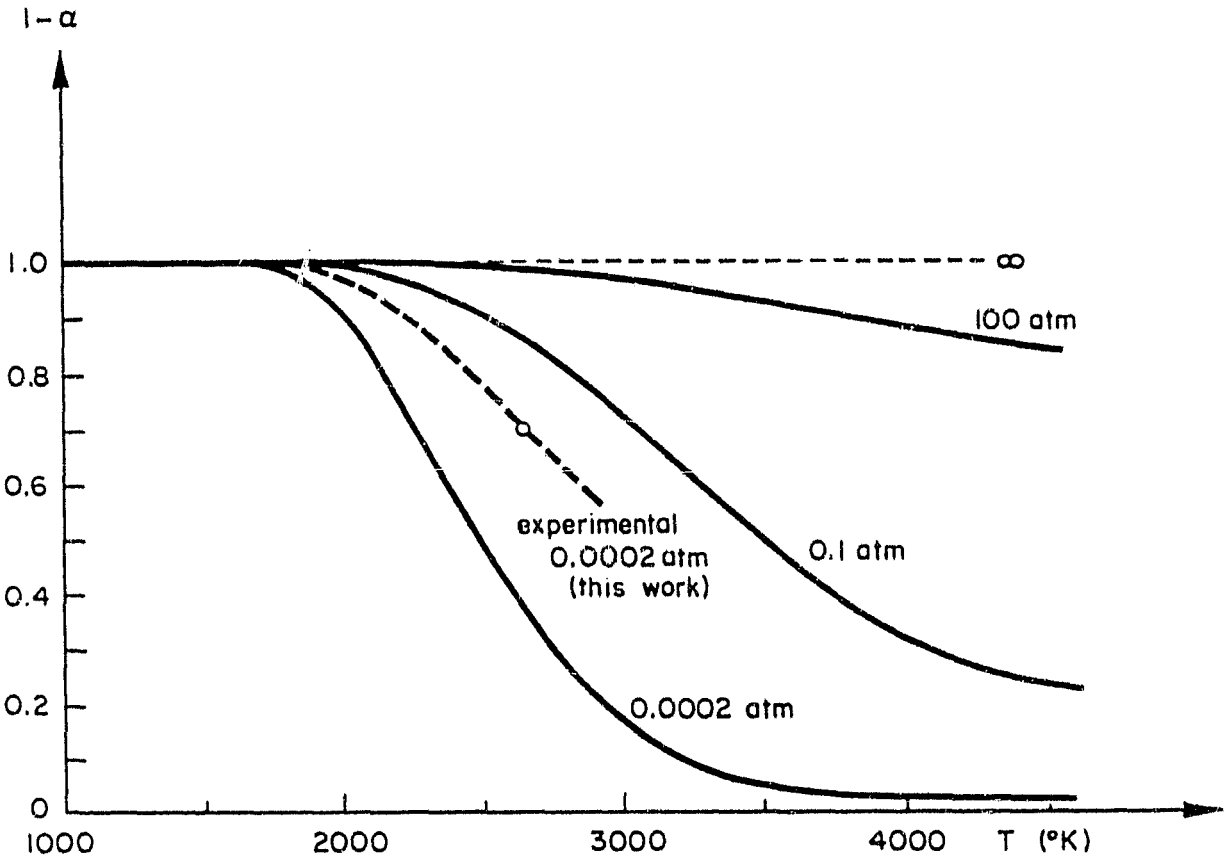

FIG. 1 DISSOCIATION DEGREE α OF WATER VAPOR AS A FUNCTION OF THE TEMPERATURE T

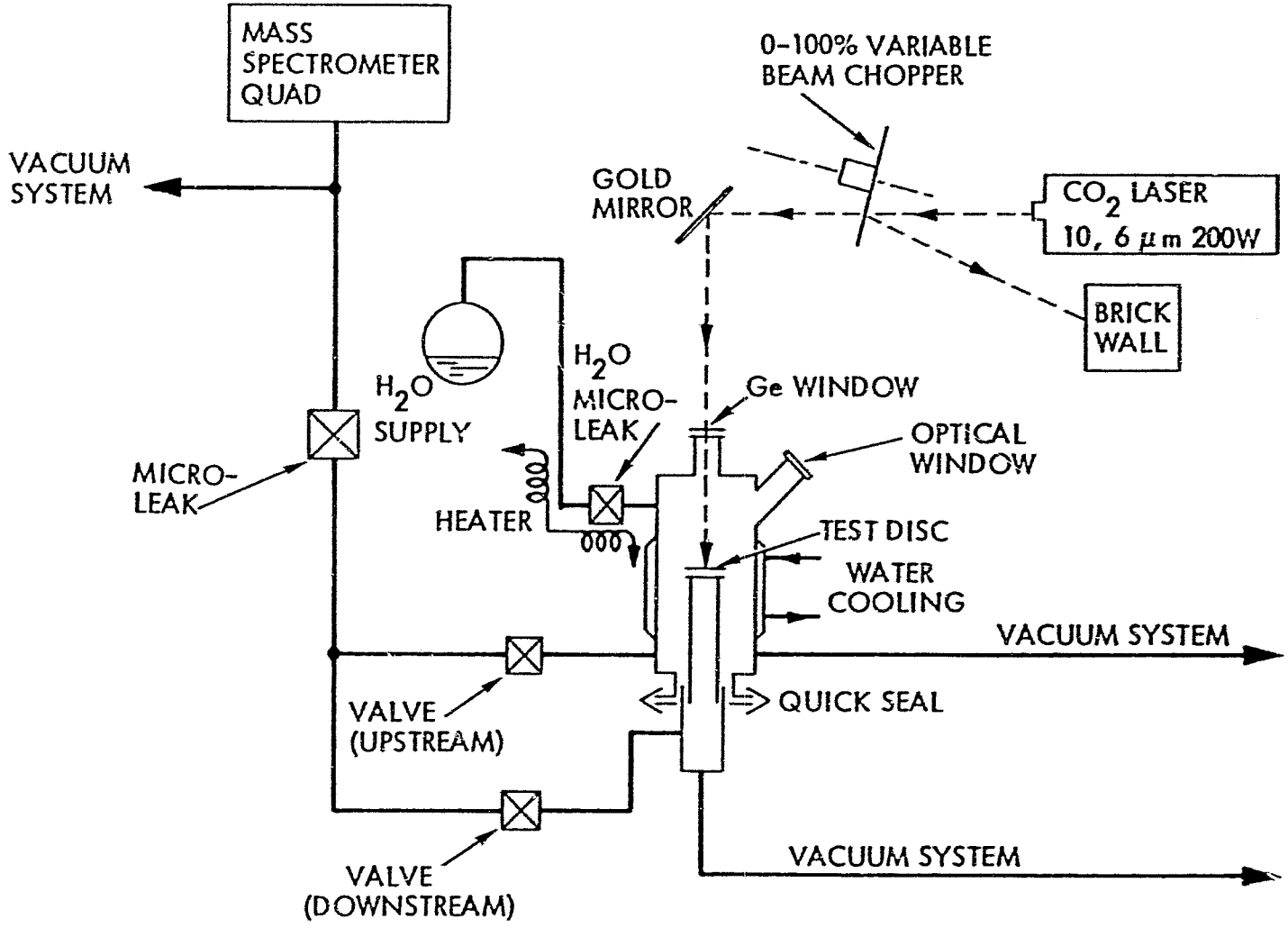

FIG. 2 - BLOCK DIAGRAM OF EXPERIMENTAL SET-UP

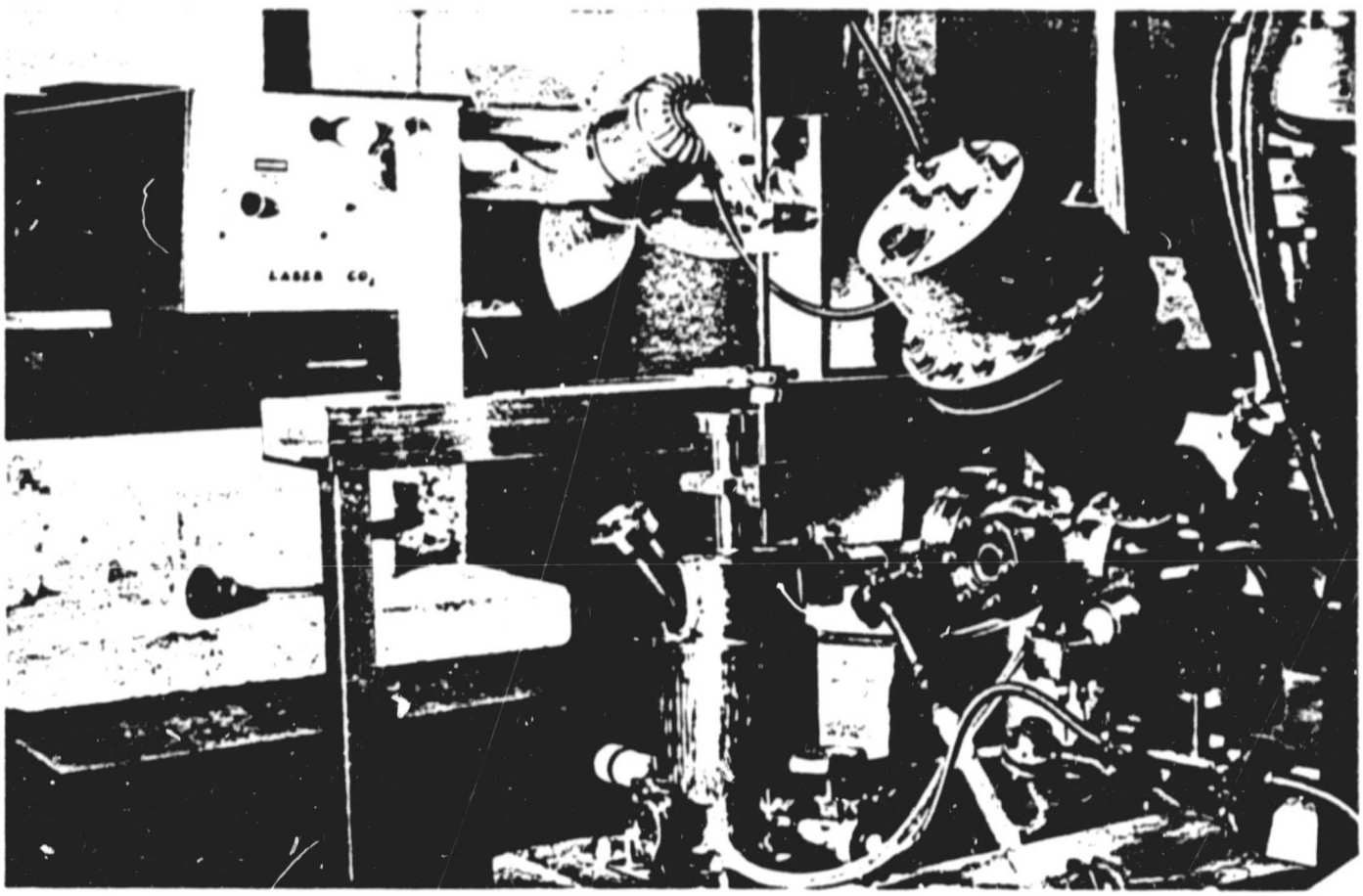

FIG. 3 - ACTUAL VIEW OF EXPERIMENTAL REACTOR

On top, to the left, is the front panel of the laser. On top, to the middle, is the chopper. On middle bottom the testing vessel can be seen. To the right, in the foreground, a disused QUAD head. The active QUAD head is visible to the extreme right of the picture, with the label "ONE". The T connection to the VARIAN microleak can be seen to the bottom right. Below the laser panel, the small instrument with a dial is the ORIEL power probel.

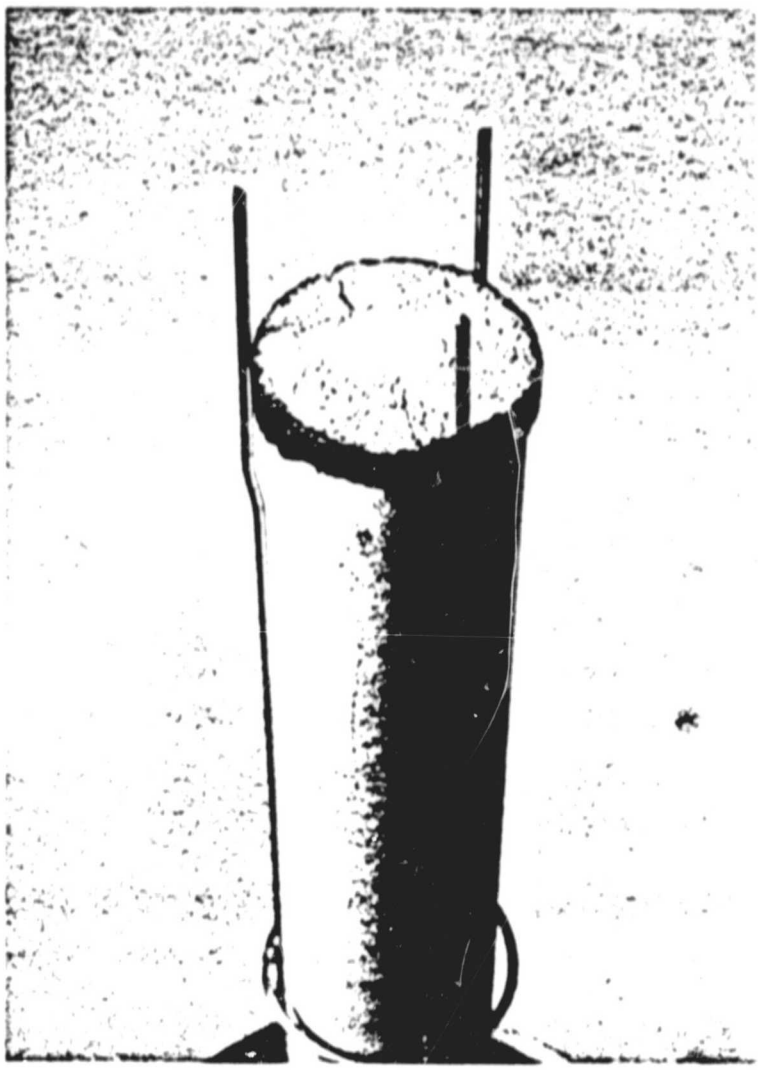

FIG. 4 - SAMPLE HOLDER

The ZrO_2 porous disc can be seen on top of the ZrO_2 compact tube. The picture shows the arrangement of three stainless steel rods which maintain the sample in its place.

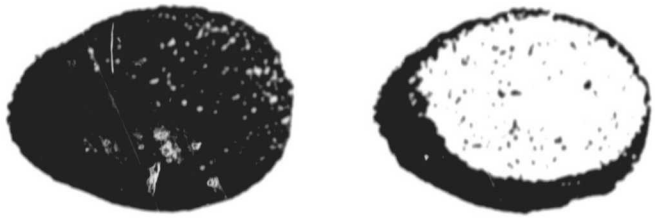

(a)

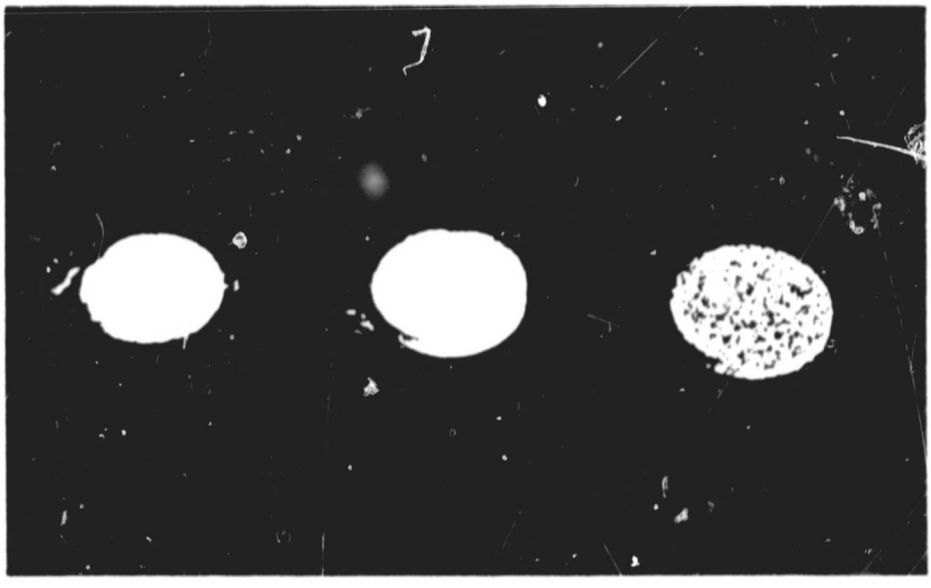

(b)

FIG. 5 - CHARACTERISTIC SAMPLES

(a) Two typical ZrO_2 discs, the left sample is as sintered. The right sample has been submitted to laser heating in air and water vapor. All the heated parts present the typical white color of fully oxidized ceramic.

(b) ThO_2 samples. To the left a first "compact" sample (without macropores) submitted to 120 W laser heating in air. The central item is a sintered sample ready for crushing. To the right, a sintered ThO_2 sample with

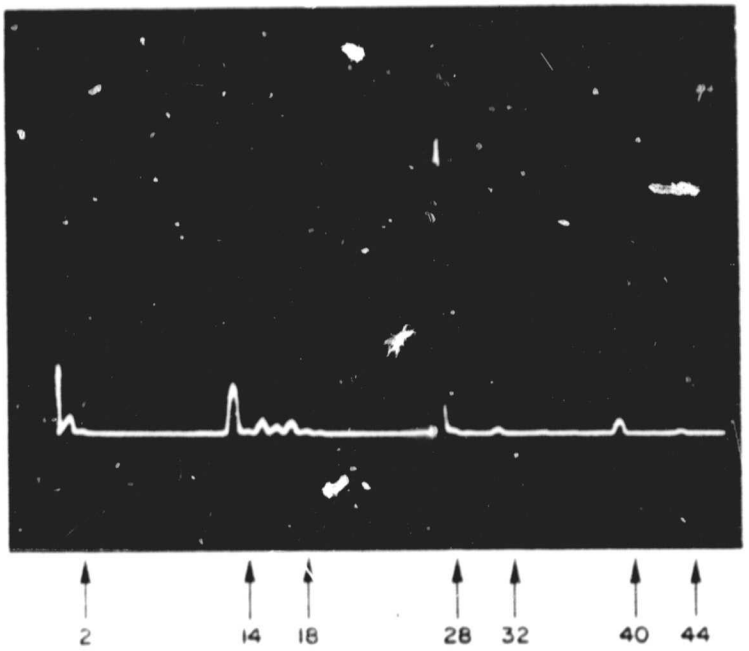

(a)
160 mV
full scale*

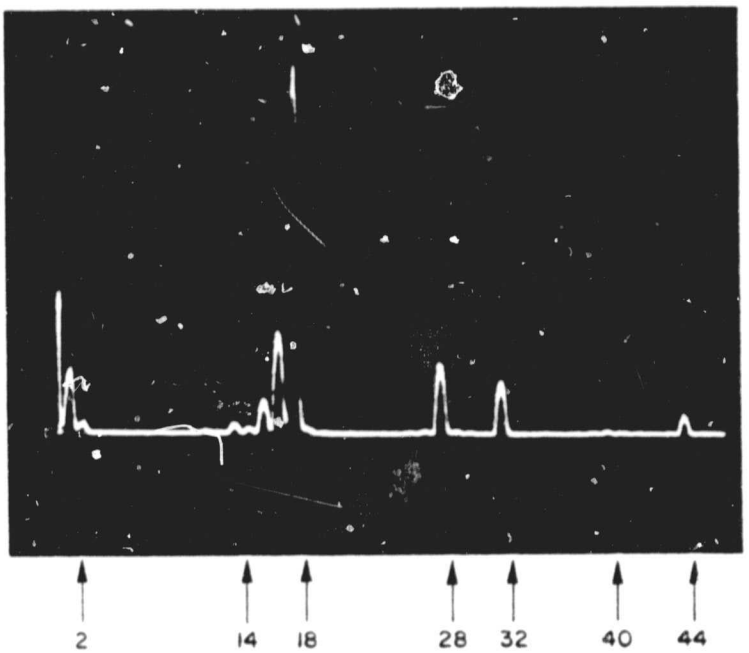

(b)
160 mV
full scale*

FIG. 6 - QUAD SPECTRA

(a) Residual air in test vessel (event 3)

(b) After H_2O introduction (event 4)

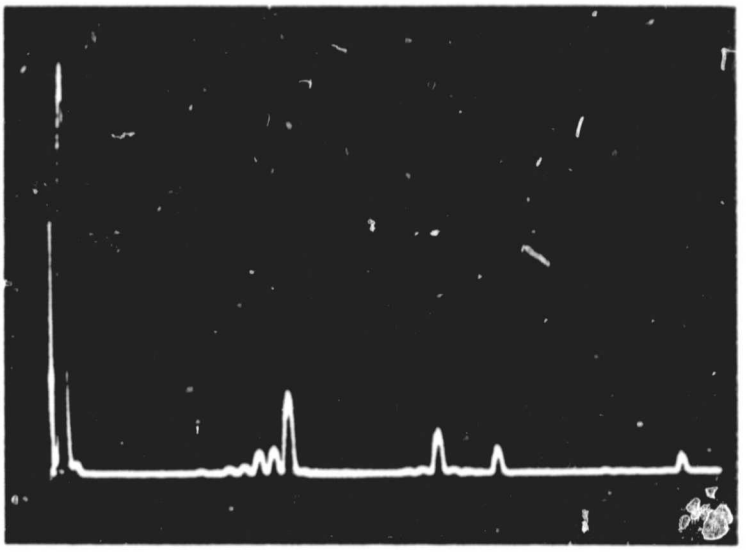

(a)
160 mV
full scale*

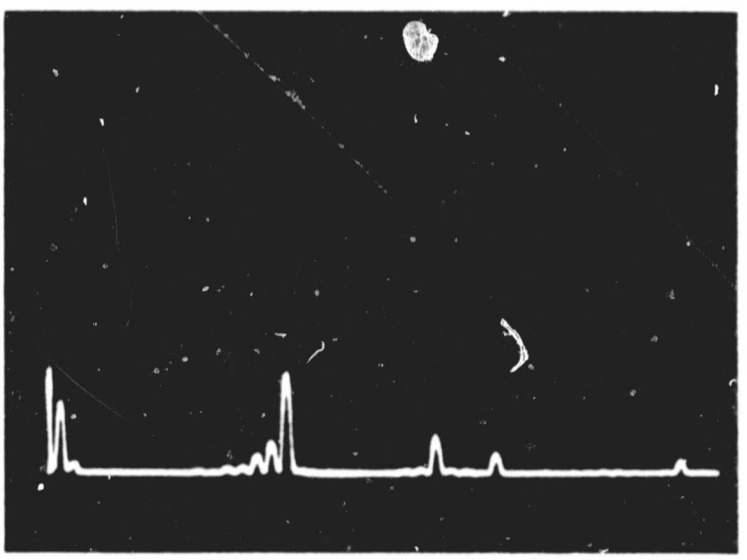

(b)
160 mV
full scale*

FIG. 7 - QUAD SPECTRA

(a) Downstream, H_2O, laser 97 W (event 15)

(b) Downstrean, H_2O, laser 19 W (event 16)

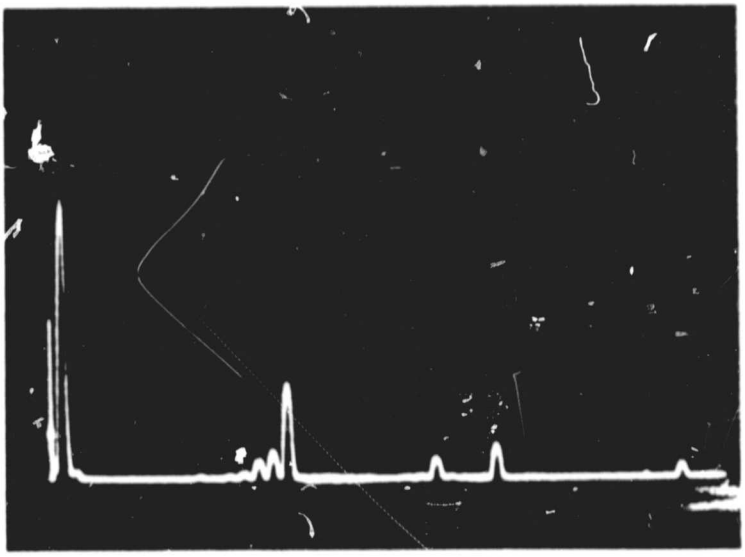

(a)
400 mV
full scale*

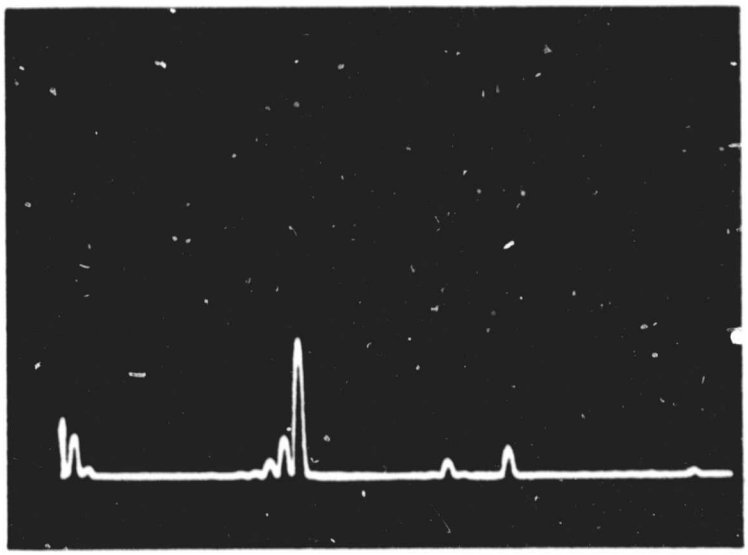

(b)
400 mV
full scale*

FIG. 8 - QUAD SPECTRA

(a) Upstream, H_2O ON, laser 91 W (event 23)

(b) Upstream, H_2O ON, laser off (event 24)

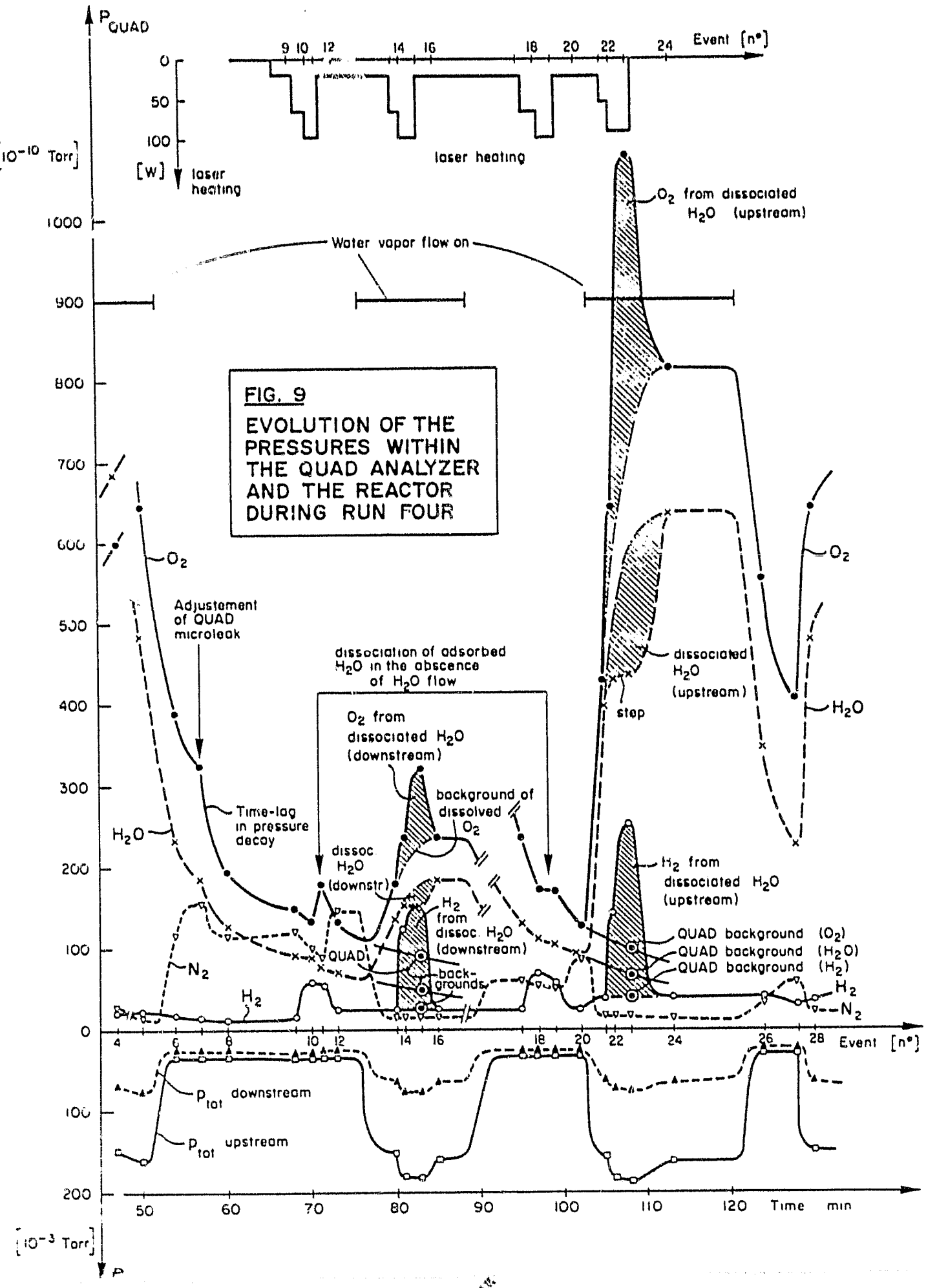

FIG. 9

EVOLUTION OF THE PRESSURES WITHIN THE QUAD ANALYZER AND THE REACTOR DURING RUN FOUR